Journal of Power Sources 254 (2014) 80–87

Contents lists available at ScienceDirect

Journal of Power Sources

journal homepage: www.elsevier.com/locate/jpowsour

Nondestructive detection, characterization, and quantification of lithium plating in commercial lithium-ion batteries

Mathias Petzl [a,*], Michael A. Danzer [a,b]

[a] Helmholtz-Institut Ulm (HIU), Albert-Einstein-Allee 11, 89081 Ulm, Germany
[b] Zentrum für Sonnenenergie- und Wasserstoff-Forschung Baden-Württemberg (ZSW), Lise-Meitner-Straße 24, 89081 Ulm, Germany

HIGHLIGHTS

- Nondestructive method to detect lithium plating in commercial Li-ion batteries.
- Differential methods enable quantification of the amount of plated lithium.
- Identification and separation of reversibly and irreversibly plated lithium.
- Simplified model for the lithium plating-stripping process.
- Extensive testing at various operating conditions elucidates the degradation process.

ARTICLE INFO

Article history:
Received 20 August 2013
Received in revised form
5 December 2013
Accepted 10 December 2013
Available online 20 December 2013

Keywords:
Lithium plating
Aging
Differential voltage analysis
Lithium stripping
Reversibility

ABSTRACT

Lithium plating is a typical aging mechanism of lithium-ion (Li-ion) batteries at low temperatures and high charge rates. Therefore an instant detection method is needed for safe battery operation and to increase the life time. Detection of lithium plating during operation is only possible by nondestructive analysis of short-term plating effects. In this study, we present a new approach to detect, characterize, and quantify lithium plating in a commercial graphite/$LiFePO_4$ battery. This is crucial for battery management systems (BMS) in real-world applications.

The method is based on a high voltage plateau in the discharge profile after charging at plating conditions. This voltage plateau corresponds to the stripping of plated lithium from the graphite surface. It is shown that differential analysis of such voltage profiles provides a quantitative estimation of lithium plating. The correlation between lithium plating and stripping necessitates a distinction of reversible and irreversible plating. Effects of various operating conditions, i.e. charge temperature, state-of-charge (SOC), and charge current, on the plating behavior are investigated in order to elucidate this degradation mode. Furthermore, the presented approach allows for determination of the reversibility of lithium plating.

1. Introduction

Metallic lithium deposition on the graphite negative electrode is one of the most severe degradation processes in modern Li-ion batteries [1–3]. This so-called lithium plating usually occurs during charging at low temperatures, high SOC and high charge rates. Other reasons are poor cell balance which can be due to aging, manufacturing failures, improper cell design or a highly resistive solid electrolyte interphase (SEI). All these factors cause high polarization of the negative electrode, i.e. poor electrode kinetics, which forces the graphite potential below 0 V vs. Li/Li^+. During low temperature charging there is a competition between intercalation of lithium ions into and lithium plating on the graphite electrode. The diffusion of lithium ions in graphite is hindered at low temperatures, which leads to a low intercalation rate and thus favors lithium plating at the graphite surface. On the other hand lithium intercalation can be impeded by charge transfer limitation which occurs at smaller time constants than the aforementioned diffusion limitation [4]. Deposited lithium exhibits different structures on the electrode surface, e.g. mossy or dendritic. Lithium dendrites may cause an internal short circuit with detrimental impact on cell safety and performance [5–7].

In general, long-term effects of lithium plating like capacity loss, decrease in coulombic efficiency and impedance rise are well-known. But they are apparently not suitable for fast detection of plating during battery operation. Thus short-term effects have to be investigated. There have been a few studies on lithium plating in Li-ion cells and the corresponding low temperature

* Corresponding author. Tel.: +49 731 9530538; fax: +49 731 9530599.
E-mail address: mathias.petzl@kit.edu (M. Petzl).

0378-7753/$ – see front matter © 2013 Elsevier B.V. All rights reserved.
http://dx.doi.org/10.1016/j.jpowsour.2013.12.060

behavior [8–10]. Harris et al. [11] investigated and modeled Li transport in a graphite electrode. Li transport properties are the key factors concerning the susceptibility of an electrode to lithium plating. In addition, various theoretical modeling approaches concerning the plating process and related phenomena were performed [12–15]. However, detailed investigations on the plating behavior of commercial Li-ion batteries are rare [16,17]. This might be due to the fact that commercial cells do not have a reference electrode which is used to measure individual electrode potentials. Detecting lithium plating by a negative graphite potential vs. Li/Li^+ is thus impossible, other strategies are needed for commercial Li-ion batteries. Smart et al. [18,19] showed an indirect evidence of lithium plating during cell operation. A high voltage plateau was observed during discharge and ascribed to the stripping of metallic lithium deposited in the previous charge step. The investigations mainly concerned the influence of electrolyte composition on lithium plating due to different SEI properties. But these studies are rather qualitative in terms of the plating reaction. For battery management systems it is important to gain quantitative information about lithium plating in order to ensure safe battery operation.

In this paper, we present a nondestructive characterization method for lithium plating which is based on the above-mentioned lithium stripping plateau. Differential analysis [20–22] of the high voltage plateau provides quantitative results concerning the stripping reaction. The correlation between plating and stripping is discussed for a better understanding of the complete deposition process. This leads to a distinction of reversibly and irreversibly plated lithium depending on the electrical contact with the graphite electrode. Charge temperature, SOC, and charge current are investigated for their effects on lithium plating. Reversibility of the plating process and coulombic efficiency can also be determined by the presented approach.

Nondestructive detection methods are crucial for online battery characterization. The aging behavior of Li-ion batteries is usually investigated by post-mortem analysis which means opening of the cell. However, this is not suitable for in situ detection of degradation processes. Moreover, post-mortem analyses lack temporal resolution of aging behavior because the results are confined to the point of cell opening.

In this study, a $LiFePO_4$-based cell is investigated in order to exclude any contributions from the positive electrode. $LiFePO_4$ exhibits a flat voltage profile [23] and negligible aging processes [24].

One cell is opened in order to confirm the deposition of metallic lithium under the investigated operating conditions.

2. Experimental

A cylindrical 26650-type commercial Li-ion battery with 2.5 Ah rated capacity (1C = 2.5 A) is investigated in this study. The cell comprises a $LiFePO_4$-based positive electrode and graphite as negative active material. According to the data sheet, cutoff voltages are 2.0 V–3.6 V and the battery can be operated down to −30 °C. Before the plating investigations the cells exhibit 98% of the initial capacity due to some prior characterization tests. The capacity is checked again after the plating tests for an estimation of the degradation effects due to low temperature charging.

Electrochemical measurements are performed on a BaSyTec CTS battery test system. The cells are stored in an ESPEC climate chamber to ensure constant temperature conditions and at least 10 h are allowed for temperature equilibration. Various operating conditions are investigated, i.e. charge temperature (−20 °C, −22 °C, −24 °C, −26 °C), SOC (1.0–0.1) and charge current (1C, C/2). Two cells are tested at each charge current for reproducibility. The detailed test procedure is described in the following. After temperature equilibration, the cells are completely discharged with a small current of C/20 in order to avoid polarization effects. A subsequent rest period of 2 h assures relaxation. Afterward full capacity (1.0 SOC) is determined by constant current–constant voltage (CCCV) charging with 1C respectively C/2, the CV phase is terminated when the current relaxes below C/20. The test system then calculates the charge amounts corresponding to 0.9–0.1 SOC. These steps, i.e. CCCV charging and C/20 complete discharging, are repeated for all SOC levels. A 2 h pause is inserted after discharging but there is no pause after the charge steps. In this way, the complete SOC range can be investigated at various charge temperatures and with different charge currents.

Differential analysis is used to derive detailed information about electrode phase properties from the discharge voltage profiles. According to Gibbs' phase rule, voltage slopes depict phase transitions and voltage plateaus indicate two-phase regions (i.e. phase equilibriums). There are two complementary methods in this context. Differential voltage (DV; dV/dQ vs. Q) provides the slope of the voltage curve [20]. Thus phase transitions are evident by peaks in a DV plot. In contrast, phase equilibriums in a voltage profile are translated into differential capacity (DC; dQ/dV vs. V) peaks [21,22]. MATLAB is used for the described methods of signal processing and data evaluation.

Cell opening is performed in a glove-box under argon atmosphere. This is due to fast reactions of the plated lithium with air. Metallic lithium is identified by water exposure afterward.

3. Results and discussion

3.1. Indirect detection of lithium plating

In Fig. 1 charge profiles of the investigated cell are shown at various low temperatures with a charge current of 1C. The voltage polarization grows with decreasing temperature which leads to short CC phases. Thus, an increasing amount of charging is achieved during the CV phases. Therefore no information about phase transitions at the graphite electrode can be derived from the charge profiles. This is due to contrary effects of operating conditions which cause the metallic lithium deposition. Lithium plating is induced by low temperatures and high charge rates. However these reduce the CC phases which contain all information on electrode phase properties. Direct detection of lithium plating is thus not possible in this case.

An indirect method for the detection of lithium plating was suggested [18,19] which uses a high voltage plateau in the discharge

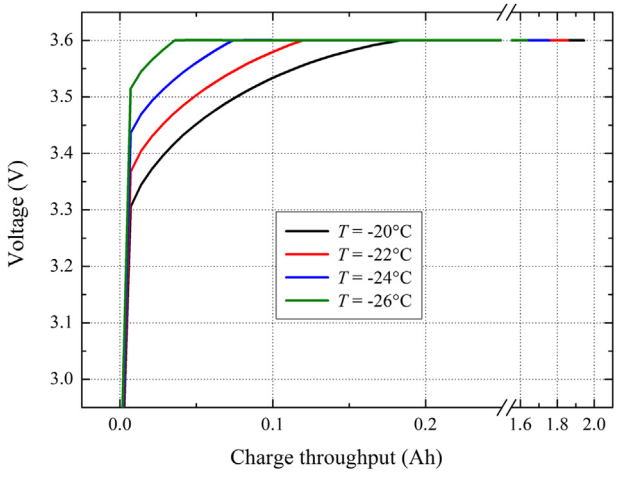

Fig. 1. Voltage profiles of charge steps to 1.0 SOC (full charge) at different temperatures with 1C charge current.

curve after charging at low temperatures. In general, voltage plateaus indicate phase transitions in the electrodes. The high voltage plateau indicates the oxidation of plated lithium, also referred to as lithium stripping, from the graphite surface. Deintercalation and lithium stripping are competing at high voltages during discharge. However, the oxidation of plated lithium is favored over lithium deintercalation. Therefore, the stripping plateau precedes the deintercalation plateaus of graphite if lithium plating has occurred. Deintercalation causes only minor capacity contributions in the region of the voltage plateau. Measurements with three-electrode cells pointed out that the stripping plateau can only be observed if the graphite potential was sufficiently negative vs. Li/Li^+. Therefore, the occurrence of the stripping plateau means that lithium plating must have happened in the previous charge step. This indirect method is applied here for the detection and quantification of lithium plating. Fig. 2 depicts discharge profiles after charging to different SOC levels at −20 °C. The stripping plateau is observed for 0.9–0.7 SOC, however it does not occur for full charge to 1.0 SOC. A detailed explanation of this behavior is given in later sections.

Fig. 3 shows a picture of the graphite electrode after cell opening under argon atmosphere. It is obvious that the surface is completely plated with a uniform layer of metallic lithium which exhibits a silver-gray color. Water contact leads to gas formation, i.e. hydrogen evolution. This confirms the occurrence of lithium plating as expected from the indirect detection.

3.2. Quantification of lithium stripping

Nondestructive methods for plating detection in commercial cells cannot use the potential of the graphite electrode due to a missing reference electrode. Thus the contributions of the positive electrode must be negligible – as it holds true for $LiFePO_4$ – in order to investigate the processes which occur at the negative graphite electrode.

DV analysis is a frequently used evaluation method for voltage profiles. Bloom et al. [20] applied DV analysis for electrode characterization and aging tests. Phase transitions are translated into DV peaks, thus electrode processes can be clearly elucidated. It is assumed that $LiFePO_4$ does not show any DV peaks due its featureless voltage behavior. Therefore, DV plots of the investigated cell offer pure information about the graphite electrode's phase properties. Usually this technique is applied to quantify different phase regions of an electrode material, e.g. intercalation stages in graphite [24]. However, lithium stripping presents an additional

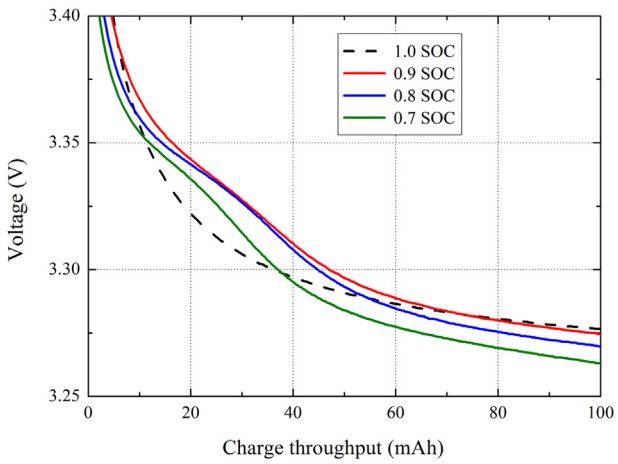

Fig. 2. Voltage profiles of discharge steps after charging to different SOC levels at −20 °C with 1C charge current.

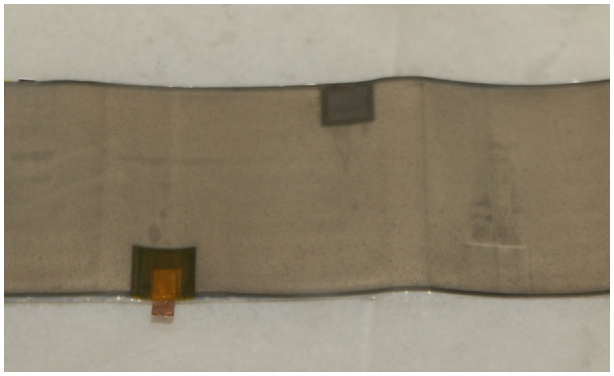

Fig. 3. Picture of the graphite electrode after cell opening under argon atmosphere.

phase transition during discharge. As mentioned above, the stripping plateau precedes the deintercalation stages of graphite. In detail, the voltage plateau which is ascribed to the stripping reaction is actually due to phase equilibrium between plated lithium and the first deintercalation stage of graphite. The DV peak is located at the point where the electrode turns single-phase again. This means that all of the (reversibly) plated lithium has been oxidized, i.e. completion of lithium stripping. In other words, the charge amount up to the DV peak is almost entirely caused by the stripping reaction. Fig. 4a shows the DV curves of the discharge profiles in Fig. 2. The observed peaks correspond to the stripping plateaus in the discharge profiles. DV analysis provides quantification of lithium stripping because the stripped charge amount $Q_{stripping}$ can be easily determined by the peak position. As discussed above (Section 3.1), deintercalation contributions are expected to be of small extent. Therefore, the determined charge amounts of lithium stripping must be considered as the upper limit. The SOC dependence of the stripping plateau and its corresponding DV peak are discussed later (Section 3.4.1).

DC analysis enables determination of the stripping voltage $V_{stripping}$. DC curves of the discharge profiles (Fig. 2) are depicted in Fig. 4b. The peak position corresponds to $V_{stripping}$ which also depends on the SOC attained in the previous charge step. $Q_{stripping}$ can be determined by integration of the DC peaks. However, it is more practicable to derive the stripped charge amount from the DV curves.

3.3. Correlation between lithium plating and stripping

For a better understanding of the plating process it is crucial to discuss the correlation between lithium plating and stripping in more detail. Previous results show that the stripped charge amount, i.e. the mass of oxidized metallic lithium, can be determined by DV analysis of the discharge profiles after charging at plating conditions. However, it remains unknown how much of the plated lithium is stripped during discharge. In other words, the reversibility of the plating process must be determined. Thus it is necessary to distinguish between reversible and irreversible plating. Reversible plating describes deposited lithium with durable electrical contact with the negative electrode. Therefore, reversibly plated lithium is stripped during the discharge step, i.e. $Q_{stripping} = Q_{rev.plating}$. This reversible part does not cause any capacity loss because it is just another way of charging the graphite electrode.

In contrast, irreversibly plated lithium exhibits only fragile electrical contact with the negative electrode. Such lithium may become electrically isolated from the graphite electrode during the stripping process. Irreversible plating, i.e. dead lithium, is thus

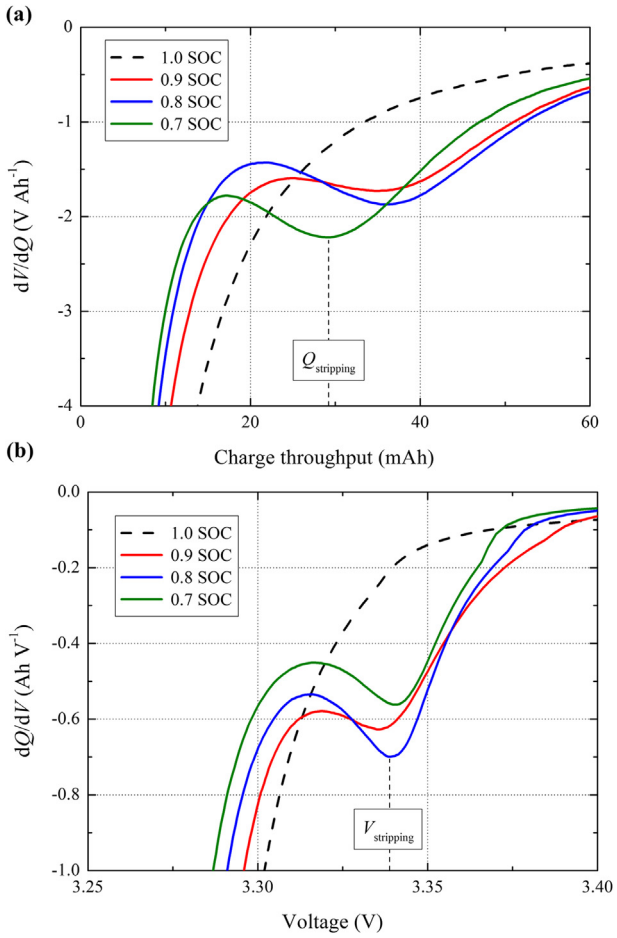

Fig. 4. (a) Differential voltage and (b) differential capacity curves of the discharge profiles in Fig. 2.

mainly responsible for the capacity losses during low temperature charging with high currents. However, there are additional capacity losses due to the formation of surface films on the plated lithium. At first lithium is plated directly on the electrode surface [25]. Reduction of lithium ions on the electrically isolating SEI is not possible. The plated lithium can grow through the SEI and get in contact with the electrolyte [16]. Subsequent surface film formation causes capacity losses which are not distinguishable from irreversible plating. Furthermore, the formation of such surface films can also cause electrical isolation of deposited lithium [4]. This means that the charge amount corresponding to irreversible plating $Q_{\text{irrev.plating}}$ includes the capacity loss caused by surface film formation. It is assumed that capacity losses due to SEI formation are negligible at low temperatures. The capacity loss during a charge–discharge cycle is simply the difference between the charge throughput during charge Q_{ch} and discharge Q_{dc}, i.e. $Q_{\text{irrev.plating}} = Q_{\text{ch}} - Q_{\text{dc}}$. This allows for determination of the complete charge amount due to lithium plating $Q_{\text{plating}} = Q_{\text{rev.plating}} + Q_{\text{irrev.plating}}$. All plating contributions are accessible by the described characterization method. The reversibility R of the plating process is now written as $R = Q_{\text{rev.plating}}/Q_{\text{plating}}$.

A plated charge amount Q_{plating} can be converted into the corresponding mass m_{plating} of plated lithium as shown in the following. The amount of lithium n_{plating} is given by $n_{\text{plating}} = Q_{\text{plating}}/F$ (Faraday constant $F = 96485.3399$ C mol^{-1} [26]) because lithium plating is a one-electron process ($Li^+ + e^- \rightarrow Li$). The mass of plated lithium m_{plating} is then calculated according to $m_{\text{plating}} = n_{\text{plating}} M_{\text{Li}}$ (molar mass of lithium $M_{\text{Li}} = 6.94$ g mol^{-1} [27]).

3.4. Effects of operating conditions on lithium plating

3.4.1. Reversible and irreversible plating

Durations of the CV phases for charging with 1C to different SOC levels at various temperatures are shown in Fig. 5. For constant temperature, the CV phase grows in an exponential manner with increasing SOC. This is due to the exponential decrease of the charge current during the CV phase (Section 3.4.2). Therefore, the duration of the CV phase must increase exponentially to attain the consecutive SOC levels. Lowering the charge temperature leads to an extension of CV phases due to strong voltage polarization (Fig. 1). Temperature and SOC dependence of the CV phase are relevant for the following discussion on reversible and irreversible plating. It is important to note that the charge current relaxes with increasing SOC during CV charging.

Fig. 6a depicts the mass of reversibly plated lithium $m_{\text{rev.plating}}$ depending on SOC and temperature (charge rate: 1C). Masses are calculated from the stripped charge amounts $Q_{\text{stripping}}$, respectively $Q_{\text{rev.plating}}$ (Section 3.3). Reversible plating increases with SOC up to a maximum at high SOC. In particular, no reversible plating can be observed at 1.0 SOC. However, it must be expected that the mass of plated lithium increases over the entire SOC range. This behavior is due to a contrary effect of charging to high SOC. It is known that reversibly plated lithium can intercalate into graphite given sufficient time [4,9,11,16,19]. The process is called chemical intercalation and becomes effective only for long CV phases, i.e. at high SOC. The amount of reversibly plated lithium is thus reduced at high SOC which leads to the observed maximum. It must be noted that the absence of reversible plating at 1.0 SOC only displays the lower limit due to the restricted sensitivity of the DV method for small lithium amounts (Section 3.4.3). As expected, reversible plating is increased with temperature reduction due to high polarization of the negative electrode, i.e. kinetic hindrance. Reversibly plated lithium is either stripped during discharge or intercalated during CV charging. Therefore, reversible plating is not responsible for capacity losses which occur during low temperature charging.

SOC and temperature dependence of irreversible plating (charge rate: 1C) are shown in Fig. 6b. The mass of irreversibly plated lithium $m_{\text{irrev.plating}}$ is calculated from the capacity loss $Q_{\text{irrev.plating}}$ during one cycle (Section 3.3). Irreversible plating exhibits only a slight increase at low SOC. An almost constant behavior is observed in this region which is unexpected because irreversible losses should vanish at low SOC. This must be due to additional capacity

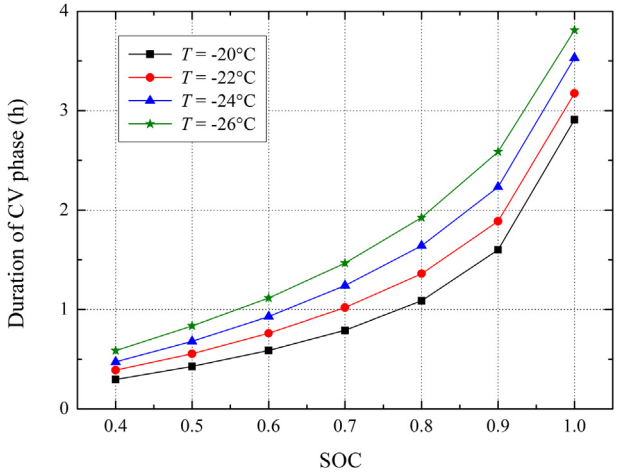

Fig. 5. Durations of the CV charge phases for different SOC levels at various temperatures with 1C charge current.

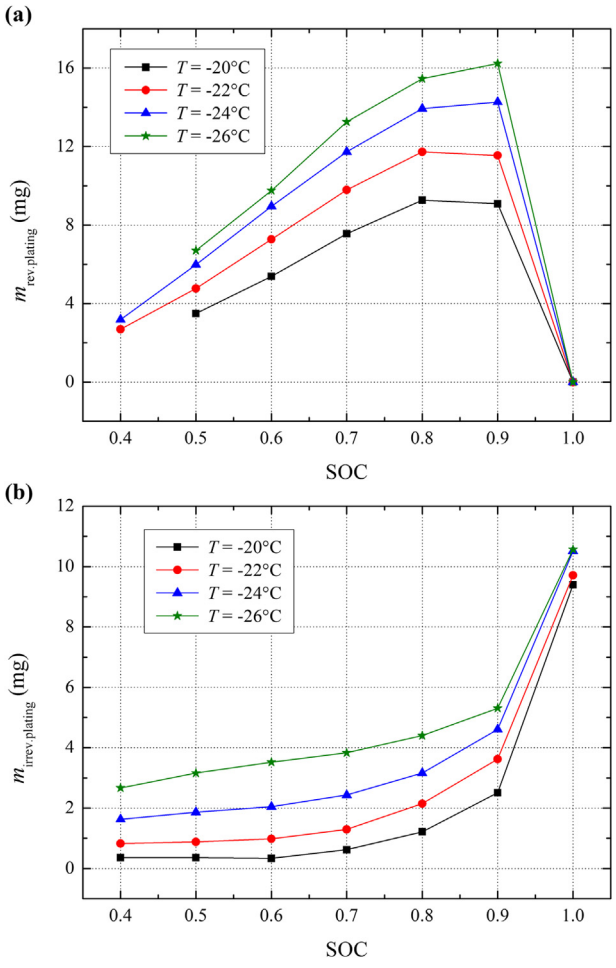

Fig. 6. SOC dependence of the mass of (a) reversibly plated lithium $m_{rev,plating}$ and (b) irreversibly plated lithium $m_{irrev,plating}$ at various temperatures with 1C charge current.

losses which are independent of SOC. It is expected that the underlying degradation mechanisms are related to lithium plating. However, the reason for this effect is still unknown. On the contrary, irreversible plating exhibits a strong increase at high SOC. This is due to surface film formation on that part of the plated lithium which has grown through the SEI during long CV phases (Section 3.4.2). Another reason is the chemical intercalation which affects the structure of the deposited lithium. The resulting porous structures can easily lose their electrical contact during the dissolution of plated lithium (Section 3.4.2). It is obvious that temperature decrease leads to more irreversibly plated lithium for constant SOC. Lower temperatures aggravate lithium plating and thus more plated lithium becomes electrically isolated during the stripping process.

3.4.2. Model of the lithium plating-stripping process

Reversibly and irreversibly plated lithium cannot be distinguished until lithium stripping during discharge. All plated lithium has electrical contact with the negative electrode up to this point because it is a condition for reductive lithium deposition. The actual capacity loss occurs during lithium stripping which causes part of the plated lithium to become electrically isolated from the graphite electrode. Results above can be explained by a simplified model of the lithium plating-stripping process which is depicted in Fig. 7 as a schematic diagram. Proportions are exaggerated for clarity reasons. The following details are neglected. Microstructural properties are not considered and the SEI is assumed to be, as an approximation, a stable and inflexible layer [28]. This model describes the SOC dependence of reversible and irreversible plating. It must be noted that the investigated deposition process is special in terms of the applied charge current. The charge current I_{ch} decreases with increasing charge time (Fig. 8), respectively SOC, during the continuous plating reaction. At low SOC, i.e. short CV phases, lithium is plated regionally with thick structure which ensures good electrical contact (Fig. 7a). High charge currents at low SOC cause much lithium to be plated in short time. This fast plating process is responsible for the dense and stable deposition structure. It is expected that high charge currents lead to the formation of relatively thick dendrites with a limited distance from the electrode surface [29]. The deposition structure at low SOC can therefore be seen as the initial stage of dendrite formation which continues at medium SOC. Moreover, the chemical intercalation of plated lithium into the graphite electrode is too slow to become significant for short CV phases. The graphite potential cannot relax sufficiently positive vs. Li/Li^+ during short CV phases so that chemical intercalation would become effective. However, this process is significant at high SOC, i.e. long CV phases. Most of the plated lithium is therefore stripped at low SOC, i.e. only minor irreversible plating (Fig. 7b). Given sufficient time at medium SOC, plated lithium grows through the SEI and gets in contact with the electrolyte (Fig. 7c). Surface films are formed immediately, leading to additional capacity losses which are indistinguishable from irreversible plating. Thus irreversible plating increases due to surface film formation and isolation of dead lithium during discharge (Fig. 7d). Chemical intercalation of plated lithium becomes effective at high SOC, i.e. long CV phases (Fig. 7e). In other words, the intercalation reaction exceeds lithium plating due to low charge currents at high SOC. This leads to a porous structure of deposited lithium near the electrode surface. Furthermore, lithium is plated more dispersed on the SEI due to low charge currents at high SOC [16]. Small charge currents correspond to slow lithium deposition and therefore lead to rather fine and fragile dendrites which are prone to electrical isolation [29]. The morphology of deposited lithium at low charge currents is also called mossy [6,25,30]. This lithium moss is described here as dispersed and porous deposition structure. Thus, surface film formation is increased due to the high surface area of the porous structures. These structures provide only deficient electrical contact. The porous lithium deposits close to the electrode surface are oxidized first during discharge (Fig. 7f). More distant lithium structures are thus easily isolated from the graphite electrode and result in dead lithium. This leads to a strong increase of irreversible plating at high SOC (Fig. 6b). Another aspect in this context is the electrical isolation of plated lithium due to surface film formation after electrolyte contact (Section 3.3). It is also possible that surface films are the main factor for the electrical isolation, i.e. formation of dead lithium.

The stripping voltage (Fig. 4b) provides additional information about the oxidation process during discharge. SOC and temperature dependence of $V_{stripping}$ are shown in Fig. 9. Apparently, this voltage only shows the potential difference between positive and negative electrode. It is however assumed that effects of the positive electrode ($LiFePO_4$) are negligible. Decreasing temperature shifts the stripping voltage to lower values for constant SOC. This is due to the slower reaction kinetics at lower temperature. The stripping voltage exhibits a maximum at medium SOC for constant temperature. A higher stripping voltage means that the lithium deposition structures at this particular SOC are more easily oxidized than the structures at another SOC with lower stripping voltage. Therefore stripping of the lithium structures at medium SOC is the most facile oxidation process. The reason for this behavior is not clear to this point and needs further investigation.

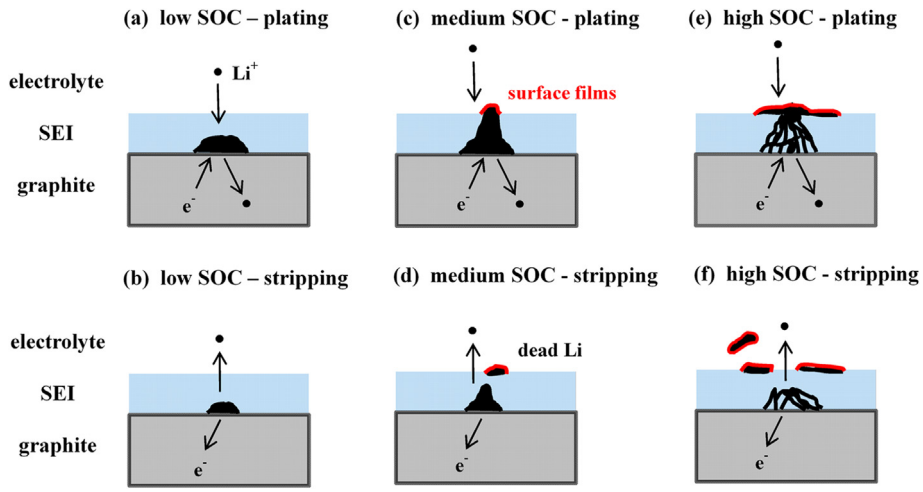

Fig. 7. Simplified model of the lithium plating-stripping process at different SOC levels: (a) plating and (b) stripping at low SOC; (c) plating and (d) stripping at medium SOC; (e) plating and (f) stripping at high SOC.

3.4.3. Growth rate and initiation point

The complete mass of plated lithium $m_{plating}$ exhibits a linear SOC dependence up to 0.8 SOC for all investigated temperatures.

Therefore linear regression of the data is performed by the method of linear least squares. Fig. 10a depicts all values for $m_{plating}$ (charge rate: 1C) and the corresponding regression curves as straight lines. The slope of the regression line corresponds to the growth rate of lithium plating. Furthermore, the initiation point of lithium plating is provided by the intercept point of the regression line with the SOC-axis. Extrapolation of the regression lines towards low SOC is reasonable due to the limited sensitivity of the presented detection method in this region. Small stripping plateaus at low SOC (≤0.3 SOC) and 1.0 SOC (Fig. 6a) cannot be detected by DV. This is due to the voltage drop at the beginning of discharge which makes small stripping plateaus and the corresponding DV peaks unidentifiable. The sensitivity is reduced with decreasing temperature because of a larger voltage drop at low temperatures.

Growth rate $\Delta m_{plating}/\Delta SOC$ (mg %$^{-1}$), initiation point (SOC), and the coefficient of determination R^2 of the linear regressions (Fig. 10a) are listed in Table 1a. 0.9 SOC is excluded from the regression due to reduced R^2 values for that case. This is caused by the flattening of the $m_{rev,plating}$ vs. SOC curves at high SOC (Fig. 6a). Growth rate values in Table 1 correspond to the mass of lithium which is deposited due to percentage SOC increase in the linear region. Table 1a shows that the growth rate increases with reduced temperature. Thus low temperature conditions do not only increase the magnitude of lithium plating but also the relative growth rate with SOC. The graphite electrode exhibits poor intercalation kinetics for lithium ions at low temperatures. This kinetic hindrance causes high polarization of the negative electrode which favors lithium plating.

The initiation point of lithium plating shifts to lower SOC with decreasing temperature, as can be seen from Fig. 10a (details in Table 1a). This means that lithium plating starts earlier, i.e. at lower SOC, when the charge temperature is reduced. Decreasing temperature leads to slow reaction kinetics of the graphite electrode which forces the potential below 0 V vs. Li/Li$^+$ at lower SOC. Another important aspect is the diffusion of intercalated lithium ions in graphite. This process becomes slower with reduced temperature which causes fast supersaturation of the lithium concentration at the graphite particle–electrolyte interfaces. Thus, plating conditions are reached at lower SOC with decreasing temperature. Fig. 10b depicts the plating behavior at a lower charge current of C/2 for comparison with 1C. The same linear dependence is observed as for the higher charge current. No plating could be detected at −20 °C with C/2 because the polarization is too small at these

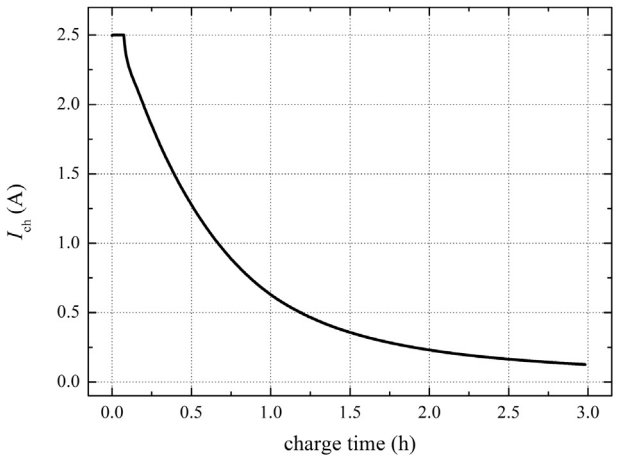

Fig. 8. Exponential decrease of the charge current I_{ch} with the increasing charge time at −20 °C.

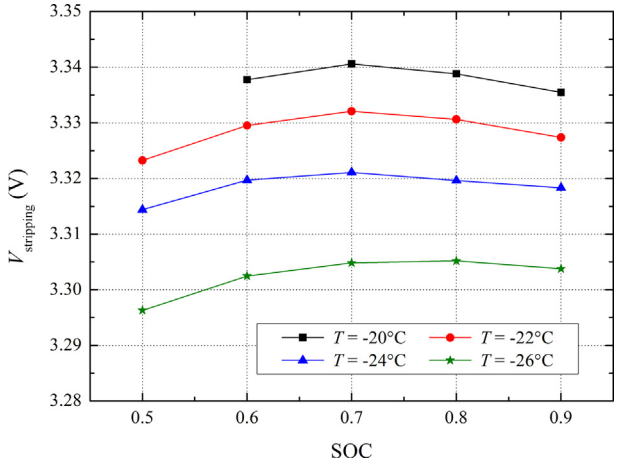

Fig. 9. SOC dependence of the stripping voltage $V_{stripping}$ at various temperatures with 1C charge current.

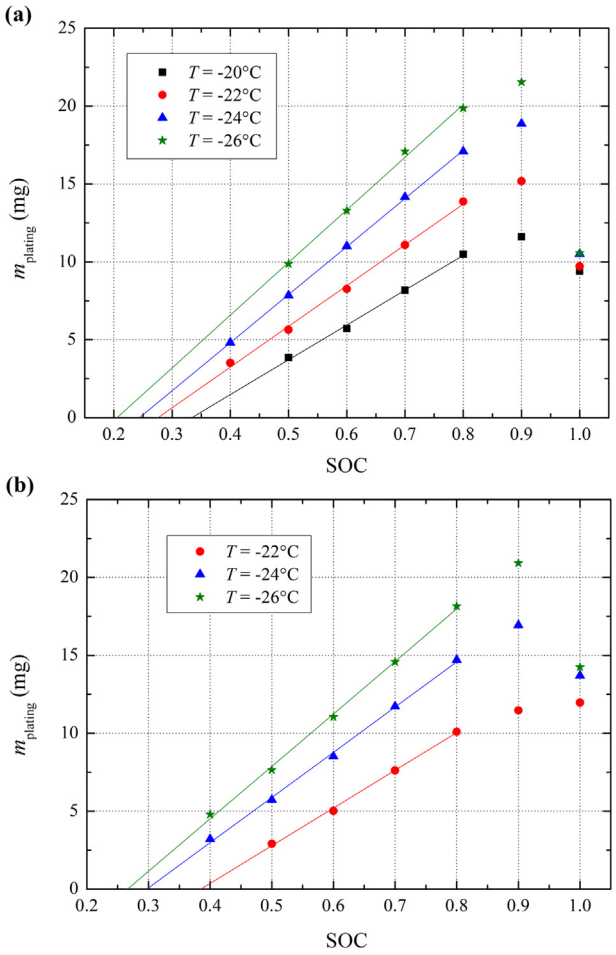

Fig. 10. SOC dependence of the complete mass of plated lithium $m_{plating}$ at various temperatures with (a) 1C and (b) C/2 charge current. Regression curves are shown as straight lines (details are listed in Table 1).

conditions to force the graphite potential below 0 V vs. Li/Li^+. At any SOC and temperature there is more lithium plating for the higher charge current except for 1.0 SOC. Lithium plating is aggravated with increasing charge currents due to higher polarization of the graphite electrode. The opposite behavior at 1.0 SOC can be explained as follows. Smaller charge currents cause relatively slow lithium deposition and thus fine plating structures (Section 3.4.2). Therefore, irreversible plating is strongly increased for C/2 at 1.0 SOC where the chemical intercalation of plated lithium is most effective. Details of the linear regressions for C/2 are listed in Table 1b. Growth rates are lower for the smaller charge current because of the discussed kinetic effects. Initiation points are located at higher SOC for the smaller charge current. Thus, plating starts later at smaller charge currents which is again due to a lower polarization. High R^2 values for all regressions support the assumption of a linear SOC dependence up to 0.8 SOC.

Table 1
Details of the linear regressions (a) with 1C and (b) with C/2 charge current: growth rate $\Delta m_{plating}/\Delta SOC$ (mg %$^{-1}$), initiation point (SOC), coefficient of determination R^2.

T (°C)	$\Delta m_{plating}/\Delta SOC$ (mg %$^{-1}$)	Initiation point (SOC)	R^2
(a)			
−20	0.2235	0.334	0.9969
−22	0.2615	0.276	0.9971
−24	0.3087	0.244	0.9998
−26	0.3379	0.205	0.9964
(b)			
−22	0.2419	0.385	0.9983
−24	0.29	0.297	0.998
−26	0.3366	0.266	0.9982

The percentage of the plated charge amount $Q_{plating}$ in the complete charge amount Q_{ch} is shown in Fig. 11 (charge rate: 1C). SOC and temperature dependence are already discussed. Fig. 11 gives an impression of the plating percentage during low temperature charging. It is obvious that the highest percentage of almost 6% is attained at the lowest temperature.

3.4.4. Reversibility and coulombic efficiency

As mentioned above (Section 3.3), the reversibility R of the plating process can be determined by the presented quantitative detection method. Fig. 12 depicts the SOC and temperature dependence of the reversibility (charge rate: 1C). The reversibility shows maxima at medium SOC for all temperatures. Decreasing reversibility towards high SOC can be explained on the basis of Fig. 7. Formation of fragile deposition structures, chemical intercalation of plated lithium, and surface film formation at high SOC lead to strong increase of irreversible plating. This is due to the resulting poor electrical pathway which causes distant structures to be isolated during lithium stripping. Such dead lithium cannot be stripped and is therefore electrochemically inactive, i.e. the reversibility is reduced. The almost constant mass of irreversibly plated lithium at low SOC (Fig. 6b) is responsible for the reversibility decrease towards low SOC. This behavior is ascribed to an unknown degradation mechanism which leads to capacity losses in addition to lithium plating. It is expected that the reversibility increases to 1.0 at low SOC without the additional degradation. The reversibility is reduced with decreasing temperature at constant SOC. Lithium plating increases at lower temperatures due to kinetic polarization effects. Thus, more plated lithium is prone to lose its electrical contact with the graphite electrode which aggravates irreversible plating and reduces the reversibility.

The coulombic efficiency CE describes the ratio between discharge and charge during one cycle, i.e. $CE = Q_{dc}/Q_{ch}$. It typically illustrates capacity losses during charging, e.g. SEI formation at ambient temperatures. CE is used here to characterize plating losses at low temperatures in a different way. Coulombic efficiency values for various SOC levels and temperatures are shown in Fig. 13. The behavior can be explained when CE is written as $CE = 1 - Q_{irrev.plating}/Q_{ch}$. Thus, the coulombic efficiency exhibits a contrary SOC dependence compared to irreversible plating for constant temperature. Coulombic efficiencies are reduced towards high SOC which is due to the strong increase of irreversible

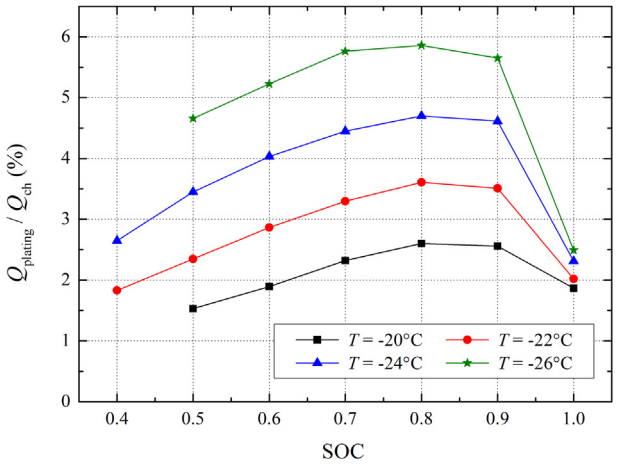

Fig. 11. Percentage of lithium plating during charging $Q_{plating}/Q_{ch}$ at various temperatures with 1C charge current.

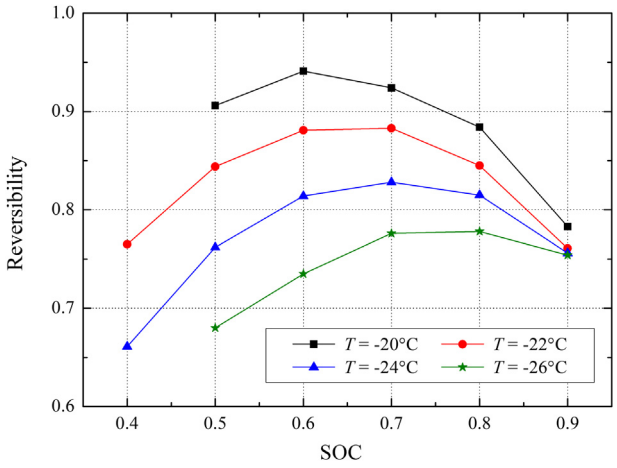

Fig. 12. SOC dependence of the reversibility *R* of lithium plating at various temperatures with 1C charge current.

plating. One would expect the coulombic efficiency to increase towards 1.0 with decreasing SOC because of only small irreversible losses. However, the constant irreversible plating at low SOC causes a decrease of coulombic efficiency. For constant SOC, decreasing temperature reduces the coulombic efficiency. This is again due to pronounced polarization of the graphite electrode which increases with temperature reduction.

4. Conclusions

In this study, a quantitative detection method for lithium plating in commercial Li-ion batteries is presented. Quantification of lithium plating is enabled by differential voltage analysis of the discharge profiles after charging at plating conditions. Further considerations result in the necessity to distinguish between different kinds of lithium plating, i.e. reversibly and irreversibly plated lithium. This distinction depends on the electrical contact of the plated lithium with the graphite electrode. In this way, it is possible to quantify the complete mass of deposited lithium during low temperature charging.

A linear SOC dependence of the plated lithium mass is observed for low to medium SOC values. Linear regression is applied for the determination of growth rate and initiation point of lithium plating. Decreasing temperature leads to higher growth rates and shifts the initiation point to lower SOC which means that the plating process starts earlier. Both results are attributed to increased kinetic effects. Our approach further allows for characterization of the plating process by other properties like reversibility and coulombic efficiency.

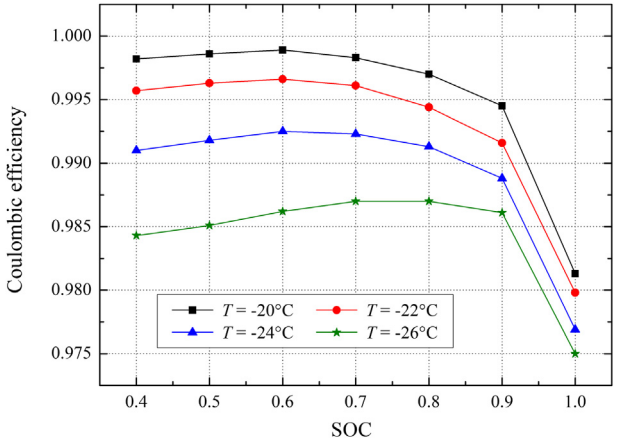

Fig. 13. SOC dependence of the coulombic efficiency CE at various temperatures with 1C charge current.

This method is suitable for all cathode materials without high potential plateaus, i.e. phase equilibriums, in the discharge profile. It is crucial that the stripping plateau is clearly identifiable and not overlain by plateaus of the cathode material.

Furthermore, the results are important for BMS in order to avoid lithium plating. A BMS for plating protection must be able to detect the stripping plateau and the corresponding DV or DC peak for an estimation of plated lithium. Afterward, the BMS can avoid lithium plating by reduction of the charge current and/or decrease of the upper SOC limit, i.e. avoiding full charge.

The capacities of the cells after the plating tests show different values depending on the charge current. The higher charge rate induces more degradation than the lower one, i.e. the cells exhibit 88% and 95% of the initial capacity. Therefore, lithium plating is aggravated with increasing charge current due to electrode polarization. The long-term aging behavior of commercial Li-ion batteries at plating conditions is subject to further studies.

Acknowledgment

This work was financially supported by Helmholtz-Institut Ulm (HIU) and Zentrum für Sonnenenergie-und Wasserstoff-Forschung Baden-Württemberg (ZSW).

The authors also want to thank Michael Kasper for the cell opening.

References

[1] P. Arora, R.E. White, M. Doyle, J. Electrochem. Soc. 145 (1998) 3647.
[2] M. Broussely, Ph. Biensan, F. Bonhomme, Ph. Blanchard, S. Herreyre, K. Nechev, R.J. Staniewicz, J. Power Sources 146 (2005) 90.
[3] J. Vetter, P. Novák, M.R. Wagner, C. Veit, K.-C. Möller, J.O. Besenhard, M. Winter, M. Wohlfahrt-Mehrens, C. Vogler, A. Hammouche, J. Power Sources 147 (2005) 269.
[4] N. Legrand, B. Knosp, P. Desprez, F. Lapicque, S. Raël, J. Power Sources 245 (2014) 208.
[5] R. Bhattacharyya, B. Key, H. Chen, A.S. Best, A.F. Hollenkamp, C.P. Grey, Nat. Mater. 9 (2010) 504.
[6] F. Orsini, A. Du Pasquier, B. Beaudoin, J.M. Tarascon, M. Trentin, N. Langenhuizen, E. De Beer, P. Notten, J. Power Sources 76 (1998) 19.
[7] F. Orsini, A. Du Pasquier, B. Beaudoin, J.M. Tarascon, M. Trentin, N. Langenhuizen, E. De Beer, P. Notten, J. Power Sources 81–82 (1999) 918.
[8] S.S. Zhang, K. Xu, T.R. Jow, J. Power Sources 115 (2003) 137.
[9] S.S. Zhang, K. Xu, T.R. Jow, J. Power Sources 160 (2006) 1349.
[10] G. Park, N. Gunawardhana, H. Nakamura, Y.-S. Lee, M. Yoshio, J. Power Sources 199 (2012) 293.
[11] S.J. Harris, A. Timmons, D.R. Baker, C. Monroe, Chem. Phys. Lett. 485 (2010) 265.
[12] M. Doyle, J. Newman, A.S. Gozdz, C.N. Schmutz, J.-M. Tarascon, J. Electrochem. Soc. 143 (1996) 1890.
[13] P. Arora, M. Doyle, R.E. White, J. Electrochem. Soc. 146 (1999) 3543.
[14] M. Tang, P. Albertus, J. Newman, J. Electrochem. Soc. 156 (2009) A390.
[15] R.D. Perkins, A.V. Randall, X. Zhang, G.L. Plett, J. Power Sources 209 (2012) 318.
[16] J. Fan, S. Tan, J. Electrochem. Soc. 153 (2006) A1081.
[17] B.V. Ratnakumar, M.C. Smart, ECS Trans. 25 (2010) 241.
[18] M.C. Smart, B.V. Ratnakumar, L. Whitcanack, K. Chin, M. Rodriguez, S. Surampudi, IEEE AESS Syst. Mag. (2002) 16.
[19] M.C. Smart, B.V. Ratnakumar, J. Electrochem. Soc. 158 (2011) A379.
[20] I. Bloom, A.N. Jansen, D.P. Abraham, J. Knuth, S.A. Jones, V.S. Battaglia, G.L. Henriksen, J. Power Sources 139 (2005) 295.
[21] A.H. Thompson, J. Electrochem. Soc. 126 (1979) 608.
[22] M. Dubarry, V. Svoboda, R. Hwu, B.Y. Liaw, Electrochem. Solid-State Lett. 9 (2006) A454.
[23] A.K. Padhi, K.S. Nanjundaswamy, J.B. Goodenough, J. Electrochem. Soc. 144 (1997) 1188.
[24] M. Safari, C. Delacourt, J. Electrochem. Soc. 158 (2011) A1123.
[25] J.-i. Yamaki, S.-i. Tobishima, K. Hayashi, K. Saito, Y. Nemoto, M. Arakawa, J. Power Sources 74 (1998) 219.
[26] P.J. Mohr, B.N. Taylor, D.B. Newell, J. Phys. Chem. Ref. Data 37 (2008) 1187.
[27] M.E. Wieser, T.B. Coplen, Pure Appl. Chem. 83 (2011) 359.
[28] Y.S. Cohen, Y. Cohen, D. Aurbach, J. Phys. Chem. B 104 (2000) 12282.
[29] C. Brissot, M. Rosso, J.-N. Chazalviel, S. Lascaud, J. Power Sources 81-82 (1999) 925.
[30] J. Wen, Y. Yu, C. Chen, Mater. Express 2 (2012) 197.